Letter

Conversion between spin and charge currents in topological-insulator/nonmagnetic-metal systems

Haoran He,[1] Lixuan Tai,[1] Hao Wu,[1] Di Wu,[1] Armin Razavi,[1] Tanay A. Gosavi,[2] Emily S. Walker,[2] Kaan Oguz,[2] Chia-Ching Lin,[2] Kin Wong,[1] Yuxiang Liu,[1] Bingqian Dai,[1] and Kang L. Wang[1,3,*]

[1]*Department of Electrical and Computer Engineering, University of California, Los Angeles, California 90095, USA*

[2]*Components Research, Intel Corporation, Hillsboro, Oregon 97124, USA*

[3]*Department of Material Science and Engineering and Department of Physics and Astronomy, University of California, Los Angeles, California 90095, USA*

(Received 27 March 2021; accepted 5 November 2021; published 22 December 2021)

The charge current in a topological insulator (TI) will induce a spin accumulation (Edelstein effect or EE), from which the spin current will be generated. Inversely, the spin current injection into the TI will induce a charge current called the inverse Edelstein effect (IEE). Some experimental and theoretical works have been done for the understanding of either EE or IEE. However, little experimental work incorporating both processes in the same TI sample has been done. In this work, we propose a phenomenological model to understand EE and IEE in the TI-based system. Based on this model, efficiencies of EE and IEE can be directly derived, which is consistent with previous theoretical work based on Boltzmann transport theory and obeying the energy conservation law. We also measure EE and IEE efficiencies experimentally in a TI/Ru/CoFeB system by spin-torque ferromagnetic resonance and spin pumping, respectively. The experimental results are consistent with our model, which proves that the spin-charge conversion in TI can be understood in the framework of (I)EE instead of (inverse) spin Hall effect. By combining theories and experiments, we find that enhancing interfacial transparency is crucial for enhancing EE efficiency, and avoiding metallic contact is crucial for enhancing IEE efficiency.

DOI: 10.1103/PhysRevB.104.L220407

The conversion between charge and spin is a central aspect of spintronics and is crucial for practical spintronic devices. Magnetization can be efficiently switched by applying an electrical current via charge to spin conversion [1–3], which can be used as a writing technique in the new generation of magnetic random-access memory. Spin to charge conversion can potentially be used to read the magnetic state, as proposed in the magnetoelectric spin-orbit (MESO) logic [4,5]. In conventional three-dimensional (3D) heavy metal (HM) systems, charge current can be converted to spin current by the spin Hall effect (SHE) [6–9] while the inverse process is called the inverse spin Hall effect (ISHE) [10]. As shown in Figs. 1(a) and 1(b), SHE and ISHE have a similar mechanism, i.e., intrinsic effect and extrinsic spin-dependent scattering. Therefore, the efficiencies for both processes are the same [11,12] and can be described by a single parameter called spin Hall angle (θ_{SH}), i.e., $J_{s,3D}/J_{c,3D} = J_{c,3D}/J_{s,3D} = \theta_{SH}$. Meanwhile, the scattering process limits $\theta_{SH} < 1$ [9].

However, experimentally, θ_{SH} in the spin to charge side and charge to spin side are not equal in some novel material systems such as the topological insulator (TI), which has the unique spin-momentum locking surface states. In the charge to spin measurement for a TI-based system, θ_{SH} can be larger than 1 at room temperature [13–18] and even as high as several hundred at cryogenic temperature [19–21]. On the contrary, θ_{SH} obtained by spin to charge measurement in similar systems is smaller than 0.1 even at 15 K [22,23]. To explain the experimental results, several groups introduced the concept of q_{EE} based on the Edelstein effect (EE) [24] and λ_{IEE} based on the inverse Edelstein effect (IEE) [25,26], which are defined in the two-dimensional (2D) system by $q_{EE} = J_{s,3D}/J_{c,2D}$, $\lambda_{IEE} = J_{c,2D}/J_{s,3D}$. Phenomenological models for either q_{EE} [24,27] or λ_{IEE} [25,28] are proposed, in which $q_{EE} \propto 1/\tau_{EE}$, $\lambda_{IEE} \propto \tau_{IEE}$, where τ_{EE} and τ_{IEE} are elusive time constants in these pioneering works. Several theoretical works [29,30] put forward the analytical expressions for q_{EE} (τ_{EE}) and λ_{IEE} (τ_{IEE}) in TI/nonmagnetic metal (NM)/ferromagnet (FM) systems based on the Boltzmann transport theory, but they did not consider the fundamental limit $q_{EE}\lambda_{IEE} < 1$ from the energy conservation law (see more discussion in the Supplemental Material [31]). Although q_{EE} and λ_{IEE} have been measured in the same Rashba system [32] and then modeled in a recent publication [33], the relation of q_{EE} and λ_{IEE} has not been measured and understood in the same TI system, which can be more important in application due to higher spin-charge conversion efficiency in TI. In addition, the spin mixing conductance between NM and FM can play an important role in τ_{EE}, which is not considered in the previous Rashba model [33].

In this work, we propose a phenomenological model incorporating both EE and IEE in a TI-based system, from which the difference between (I)EE and (I)SHE can be distinguished. Besides, the expressions for $q_{EE}(\tau_{EE})$ and $\lambda_{IEE}(\tau_{IEE})$ can be directly derived; they are consistent with previous theoretical work based on the Boltzmann transport theory and obey the energy conservation law. Experimentally, we employ a $(Bi, Sb)_2Te_3$/Ru/CoFeB film stack and measure λ_{IEE} and q_{EE} through two standard methods: spin pumping and spin-torque ferromagnetic resonance (ST FMR), respectively. τ_{EE} and τ_{IEE}

*wang@ee.ucla.edu

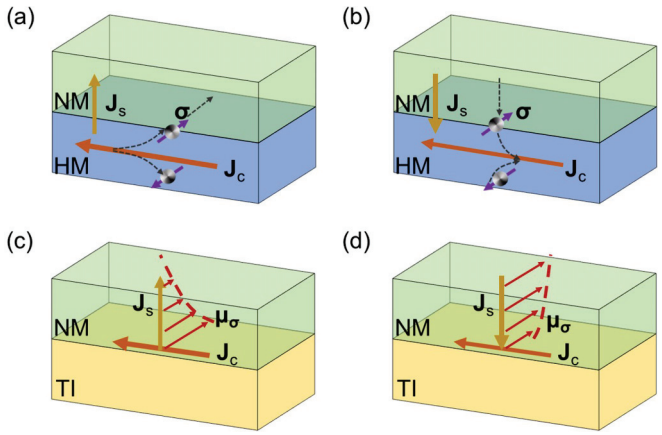

FIG. 1. (a,b) Schematics for the spin Hall effect (SHE) and inverse spin Hall effect (ISHE) in a heavy metal (HM) attached to another nonmagnetic metal (NM). SHE and ISHE are both based on spin-dependent scattering. When electrons with spin polarization $\boldsymbol{\sigma}$ get a velocity due to electrical or spin potential, they will be scattered into the orthogonal direction. (c,d) Schematic for the Edelstein effect (EE) and inverse Edelstein effect (IEE) in a topological insulator (TI) attached to a NM. Spin-momentum locked surface states in the TI lead to a one to one correspondence between charge current $\boldsymbol{J}_c$ in TI and spin potential at the TI interface $\boldsymbol{\mu}_\sigma$. Spin currents $\boldsymbol{J}_s$ are related to $\boldsymbol{\mu}_\sigma$ by scattering and diffusion processes. Therefore, EE and IEE can be understood by two independent steps: intrinsic spin-momentum locking and extrinsic spin diffusion.

are obtained and turn out to be consistent with our model. Our work provides a platform to understand ultrahigh θ_{SH} in some systems and guides the way to increase either q_{EE} or λ_{IEE} for potential applications.

Figures 1(c) and 1(d) show the schematic for EE and IEE in TI/NM, respectively. Spin-momentum locked surface states in TI lead to a one to one correspondence between 2D charge current $\boldsymbol{J}_c$ in TI and accumulated spin-polarized electrons Δn (or spin potential at TI interface $\boldsymbol{\mu}_\sigma$). The unique correspondence between spin and charge comes from intrinsic properties of TI band structure, and it can be directly derived, $\boldsymbol{J}_c = e\Delta n v_F$ [25], where v_F is the Fermi velocity. On the other hand, 3D spin current $\boldsymbol{J}_s$ strongly depends on the electron tunneling across the TI/NM interface and the diffusion process in the adjacent NM layer. Therefore, the conversion between Δn and $\boldsymbol{J}_s$ comes from the extrinsic properties of TI and is governed by the continuity equation, $\boldsymbol{J}_c = e\Delta n/\tau$, where τ is the time constant for spin transport. Note that τ is different in EE and IEE due to different spin potential distribution as shown in Figs. 1(c) and 1(d). In the EE case, Δn is fixed and spin current comes from the diffusion process. To get the spin current, the spin-polarized electrons need to overcome the potential barrier at the TI/NM interface and then diffuse into the NM layer. As a result, two series processes are involved so that $\tau_{EE} = \tau_t + \tau_{sf}$, where τ_t represents electron tunneling time across the TI/NM interface and τ_{sf} represents the spin-flip time. Note that τ_{sf} plays a role in the spin current generation since the spin current is generated by the gradient of extra spin. If NM has infinite τ_{sf}, spin diffusion length will also be infinite which leads to zero spin currents. In the IEE case, the spin current source continuously injects extra carriers into the TI interface, which must be scattered out in the equilibrium state. There are two independent channels for such scatterings: in the TI band or tunneling into the NM layer. Therefore, $1/\tau_{IEE} = 1/\tau_{TI} + 1/\tau_t$ as a parallel circuit or a set of two parallel events, where τ_{TI} represents the scattering time within TI band structure. Combining all the above arguments, the following equations can be derived directly:

$$q_{EE} = \frac{1}{v_F(\tau_t + \tau_{sf})}, \tag{1}$$

$$\lambda_{IEE} = \frac{v_F}{\frac{1}{\tau_{TI}} + \frac{1}{\tau_t}}. \tag{2}$$

Note that Eqs. (1) and (2) here, which are simply derived from the physical model, have a very similar form compared with equations derived previously from more detailed Boltzmann transport theory [29,30]. Equation (1) is the same as Ref. [29], while Eq. (2) has the same physical meaning but differs by a factor of 2 compared with the equations in Ref. [30] (see additional discussions in the Supplemental Material [31]). Although more detailed theoretical study still needs to be explored in the future for further understanding, in general, our simple physical model captures the main features and is consistent with the previous theory. Also, the product of q_{EE} and λ_{IEE} is always smaller than 1 by multiplying Eqs. (1) and (2), which originates from the energy conversion law. If we suppose $q_{EE}\lambda_{IEE} > 1$, by putting two such materials together and applying electrical current, the infinite spin-charge conversion loop with amplification between two materials will finally induce an infinite electrical current, which is wrong. The above arguments in principle are not limited to the TI/NM case but also applicable to other TI/nonmagnetic insulators and TI/FM cases. For the TI/nonmagnetic insulator case, electrons tunneling into the insulator is almost forbidden, so τ_t is very large. As a result, q_{EE} will approach zero but λ_{IEE} will be larger compared with the TI/NM case. For the TI/FM case, one major concern is that the band structure of TI may be significantly changed by the exchange interaction, as suggested in the α-Sn/Fe case [25]. However, the similar phenomenon seems not to happen in the Bi_2Se_3 [13] and BST [18], which can still give a large q_{EE}, even directly contacting with FM.

Above we only discuss the situation for bilayer cases. Experimentally, trilayer system TI/NM/FM stacks are more often studied since the FM is essential for spin current generation and detection as well as application. In the trilayer case, NM thickness is much smaller than the spin diffusion length so that the spin potential can be considered as a step function across the NM/FM interface. The spin-flip process will happen in the NM/FM interface instead of NM bulk so τ_{sf} should be replaced by an effective time constant τ_{mix} across the NM/FM interface, i.e.,

$$q_{EE} = \frac{1}{v_F(\tau_t + \tau_{mix})}. \tag{3}$$

Also, τ_{mix} has a simple relation with spin mixing conductance $g^{\uparrow\downarrow}_{mix}$ in the NM/FM interface:

$$\tau_{mix} = \frac{\pi\hbar N_F}{g^{\uparrow\downarrow}_{mix}} \tag{4}$$

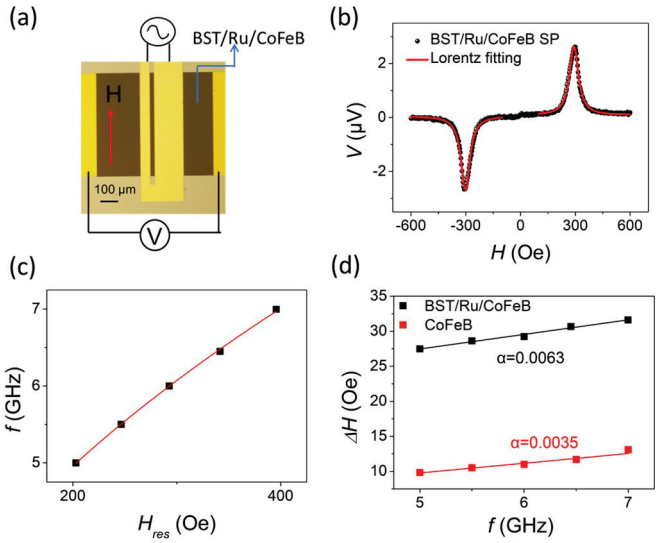

FIG. 2. Room temperature spin pumping setup and results. (a) An optical micrograph of the actual fabricated device. (b) Spin pumping voltage signal at 6.5 GHz, 16 dBm for BST/Ru/CoFeB and SiO_2/CoFeB. (c) Resonance frequency for BST/Ru/CoFeB as a function of the magnetic field, which can be fitted well by the Kittel equation. (d) Half width at half maximum ΔH as a function of frequency for the BST/Ru/CoFeB and the SiO_2/CoFeB, respectively. The damping constant α is obtained from the slope by linear fitting.

where N_F represents the density of state of Ru at the Fermi level projected into 2D [29]. From Eqs. (3) and (4), it is clear that a higher $g^{\uparrow\downarrow}_{\rm mix}$ will give a higher charge to spin conversion efficiency, as expected. The above expressions for $\tau_{\rm EE}$ and $\tau_{\rm IEE}$ are also applicable for the Rashba 2D system, while Ref. [33] did not consider the influence of $\tau_{\rm mix}$, which is the major difference between our model and their model.

To further confirm the model as well as to measure these time constants, we conduct experiments in the $(Bi, Sb)_2Te_3$ (BST)/Ru/CoFeB system. Six quintuple layers of BST were grown on Al_2O_3 (0001) substrates by molecular beam epitaxy, and then Ru(5 nm)/CoFeB(5 nm)/MgO(2 nm)/Ta(2 nm) multilayers were deposited by magnetron sputtering. Spin pumping is a standard method to determine spin to charge conversion efficiency in HM [10,34,35], TIs [22,23,36,37], or other Rashba material systems [26,38] via ferromagnetic resonance (FMR). The device geometry and measurement setup are shown in Fig. 2(a). Here, an additional 50 nm of AlO_x is grown to insulate the samples and the coplanar waveguide. Figure 2(b) shows the room temperature spin pumping result for BST/Ru/CoFeB and the reference sample SiO_2/CoFeB at the frequency of 6.5 GHz. The signal in the reference sample originates from the thermal effect [39] (see the Supplemental Material [31] for more detail), while the signal in the BST/Ru/CoFeB has the opposite sign, which comes from spin pumping. Figure 2(c) shows the resonant field $H_{\rm res}$ as the function of microwave frequency f, which can be fitted well by the Kittel formula $f = \frac{\mu_0\gamma}{2\pi}\sqrt{H_{\rm res}(H_{\rm res}+M_{\rm eff})}$ with $\gamma = 1.9\times10^{11}$ (T^{-1} s^{-1}) and $\mu_0 M_{\rm eff} = 1.35$ T. A half width at the half maximum (HWHM) ΔH can be fitted by $\Delta H = H_0 + 2\pi f\alpha/(\gamma\mu_0)$ as shown in Fig. 2(d), from which the values of Gilbert damping constant α for the BST/Ru/CoFeB and SiO_2/CoFeB are obtained from the slopes around 0.0063 and 0.0035, respectively. The enhanced damping $\Delta\alpha$ for the TI-based sample can be the evidence for spin pumping [40], but may also originate from the quality difference in the CoFeB. The latter one is hard to separate and will induce minor errors in the estimation of the spin mixing conductance (see additional experiments and discussions in the Supplemental Material [31]). The effective spin mixing conductance of the whole system $g^{\uparrow\downarrow}_{\rm eff}$ can be evaluated by $g^{\uparrow\downarrow}_{\rm eff} = \frac{4\pi M_s t_{\rm CoFeB}}{g\mu_B}\Delta\alpha$, where $t_{\rm CoFeB}$ is the thickness for CoFeB, M_s is the saturation magnetization, g is the Landé g factor, and μ_B is the Bohr magneton. $g^{\uparrow\downarrow}_{\rm eff}$ in our system is estimated around 9×10^{18} m^{-2}, comparable with the result in TI/NiFe [22,36]. The spin current density (in A/m^2) generated at resonance can be described as $J_s = \frac{e g^{\uparrow\downarrow}_{\rm eff}\omega^2 {h_{rf}}^2}{4\pi\Delta H^2}\frac{\mu_0 M_{\rm eff}\gamma+\sqrt{(\mu_0 M_{\rm eff}\gamma)^2+4\omega^2}}{(\mu_0 M_{\rm eff}\gamma)^2+4\omega^2}$ [35], where e is the electron charge, $\omega = 2\pi f$, and $h_{\rm rf}$ is the microwave magnetic field amplitude ($\sim$1.7 Oe) at 6.5 GHz. The spin current can generate charge current via IEE and induce an open circuit voltage $V = J_s\lambda_{\rm IEE}RW$, where R is the total sheet resistance shunted by metal, 55 Ω for the sample; W is the effective length of the device. Thus, $\lambda_{\rm IEE} \sim 0.091$ nm for our BST/Ru/CoFeB sample, which is comparable with previous reports [22,36,39].

ST FMR is commonly used to evaluate the charge to spin efficiency for HM [41] or TI [13,24], which is also based on FMR. However, different from spin pumping described before, here the microwave current is directly injected into the devices, which induces additional spin-orbit torque besides the Oersted field. We applied this technique for BST/Ru/CoFeB, as shown in the schematic of Fig. 3(a). Figure 3(b) shows the room temperature ST FMR signal measured at 6.5 GHz, which can be fitted well by a symmetric part and an antisymmetric part [41], $V = S\frac{\Delta H^2}{\Delta H^2+(H-H_{\rm res})^2} + A\frac{\Delta H(H-H_{\rm res})}{\Delta H^2+(H-H_{\rm res})^2}$, where S and A represent the coefficient of the symmetric part and the antisymmetric part, respectively. The symmetric part comes from the spin torque (damping-like torque) from TI, which is proportional to the 2D current density in the TI surface state while the antisymmetric part is dominated by the Oersted field, which is determined by the current density in the Ru layer due to its low resistivity. Note that the fieldlike torque can be ignored by comparing the sample with and without BST (see the Supplemental Material [31]). The value of $q_{\rm EE}$ can be expressed as $q_{\rm EE} = \frac{R_S}{R_{\rm Ru}}\frac{S}{A}\frac{e\mu_0 M_s t_{\rm CoFeB}}{\hbar}\sqrt{1+(M_{\rm eff}/H_{\rm res})}$ [24,41], where $R_{\rm Ru}$, R_S represent the sheet resistance of Ru and the topological surface state. We can obtain $q_{\rm EE}$ at different frequencies in Fig. 3(c) with the assumption that TI bulk is perfectly insulating and the top and bottom surfaces have the same resistance. For comparison with the literature, we also get the value of $\theta_{\rm SH}$ in Fig. 3(c) by treating BST like a uniformly conducting 3D HM. Note that numerically, $\theta_{\rm SH} = q_{\rm EE}t_S$, where t_s is 3 nm, half of the TI thickness. In Fig. 3(c), $q_{\rm EE}$ is almost constant at different frequencies, and the average value is 0.45 ± 0.06 nm^{-1} ($\theta_{\rm SH} = 1.35\pm0.18$), which is comparable to the previous results measured by ST FMR [13,24] or harmonic methods [16,17] at room temperature.

The temperature dependence of $\lambda_{\rm IEE}$, $q_{\rm EE}$, and $g^{\uparrow\downarrow}_{\rm eff}$ is obtained and shown in Figs. 4(a)–4(c), respectively. $\lambda_{\rm IEE}$

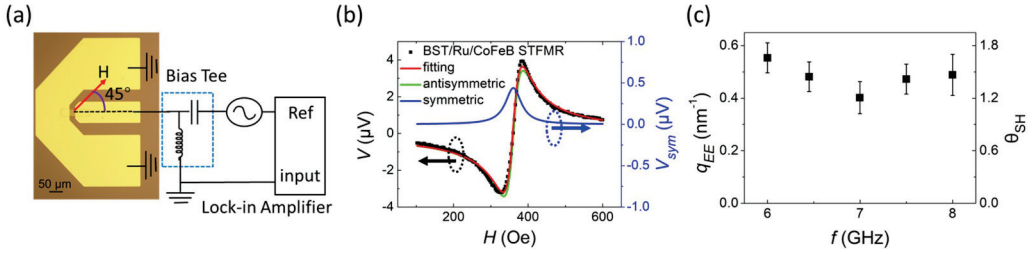

FIG. 3. Room temperature ST FMR. (a) Schematic of ST FMR measurement for a BST/Ru/CoFeB system. (b) ST FMR signal for the BST/Ru/CoFeB at 6.5 GHz which can be fitted well by a symmetric part (refer to the right axis) plus an antisymmetric part. (c) Charge to spin conversion efficiency q_{EE} (defined in 2D) and θ_{SH} (defined in 3D) are almost independent of frequency. $\theta_{SH} > 1$ at all frequencies, which suggests the 3D model cannot explain the data.

increases with decreasing the temperature while q_{EE} rapidly increases when the temperature drops to 250 K and remains almost constant down to 77 K. Note that q_{EE} is underestimated above 230 K due to the shunting of bulk carriers at high temperature (see TI resistance as a function of temperature in the Supplemental Material [31]). The data in Figs. 4(a) and 4(b) could not be interpreted by the 3D model for two reasons. Firstly, $\theta_{SH} > 1$ in the temperature range we measured. Secondly, in the SHE model, the spin diffusion length λ_{sd} is around $\lambda_{IEE}/\theta_{SH}$ [25], which is lower than 0.1 nm for all the temperatures. Such an ultrashort spin diffusion length does not make sense. Also, this 0.1 nm is more than one order of magnitude smaller than HM [34], and even smaller than some oxides such as $SrTiO_3$ [42]. Therefore, our experimental results should be understood in the 2D model, where Eqs. (2) and (3) are applied (note that the spin diffusion length of Ru is much thicker than 5 nm [43]).

In the BST/Ru/CoFeB system, v_F and τ_{TI} are intrinsic parameters of BST, whose values are reported around 3.7×10^5 m/s [44] and 1 ps [45], respectively. Since metallic states are involved in terms of τ_t and τ_{mix}, both time constants are in the femtosecond range. With the condition $\tau_{TI} \gg \tau_t$, Eq. (2) can be simplified to

$$\lambda_{IEE} \sim v_F \tau_t. \tag{5}$$

Combining Eqs. (3) and (5) as well as q_{EE} and λ_{IEE} at different temperatures, τ_t and τ_{mix} can be obtained and plotted in Fig. 4(d). Note that if the τ_{mix} term is ignored, q_{EE} λ_{IEE} $\sim$1, which is far away from our experimental result. On the contrary, the τ_{mix} term in our system turns out to dominate the charge to spin conversion since $\tau_{mix} > 10\tau_t$. τ_t slightly increases as the temperature decreases, while τ_{mix} remains almost constant. Meanwhile, the relation between measurable $g_{eff}^{\uparrow\downarrow}$ and $g_{mix}^{\uparrow\downarrow}$ can be derived analytically based on Eq. (2) and Refs. [29,30] (see the Supplemental Material [31] for the derivation):

$$g_{eff}^{\uparrow\downarrow} = g_{mix}^{\uparrow\downarrow} \frac{\tau_{sf}}{\tau_{sf} + 4\tau_t} \sim g_{mix}^{\uparrow\downarrow}. \tag{6}$$

Combining Eqs. (4) and (6), $\tau_{mix} \sim \frac{\pi \hbar N_F}{g_{eff}^{\uparrow\downarrow}}$ (7) is obtained, which gives the relation between two independently measured parameters $g_{eff}^{\uparrow\downarrow}$ and τ_{mix}, so it can be used to verify our model. It turns out these equations can match our data well. Firstly, both $g_{eff}^{\uparrow\downarrow}$ and τ_{mix} are almost constant from 77 to 250 K as shown in Figs. 4(c) and 4(d). Secondly, using the N_F value from the first principle calculation [46] and $g_{eff}^{\uparrow\downarrow}$ we measured, Eq. (6) gives τ_{mix} around 8.7 fs, which is not far from the value ($\sim$3.8 fs) we obtained. τ_t and τ_{mix} are both spin tunneling time across the interface, so in principle, they should both be temperature independent. Experimentally, an almost constant τ_{mix} and weak temperature-dependent τ_t are observed, which is close to the expected results, though more study is still needed to further understand the different temperature dependences of them.

Finally, we want to discuss the potential application for TI in spintronics based on our model. Fundamentally, a TI or 2D system has limitations on the product of q_{EE} and λ_{IEE} but may not have a limit on either q_{EE} or λ_{IEE}, which suggests a 2D system can potentially have ultrahigh charge to spin or spin to charge conversion efficiency, while in 3D SHE material $\theta_{SH} < 1$ from both sides. Different strategies should be used to enhance q_{EE} and λ_{IEE}. For enhancing q_{EE}, $\tau_{mix} + \tau_t$ should be reduced. Since in our BST/Ru/CoFeB system $\tau_{mix} \sim 10\tau_t$, reducing τ_{mix} (or increasing $g_{mix}^{\uparrow\downarrow}$) at the NM/FM interface may be more crucial compared with reducing τ_t at the TI/NM interface, which converts the complicated TI interface

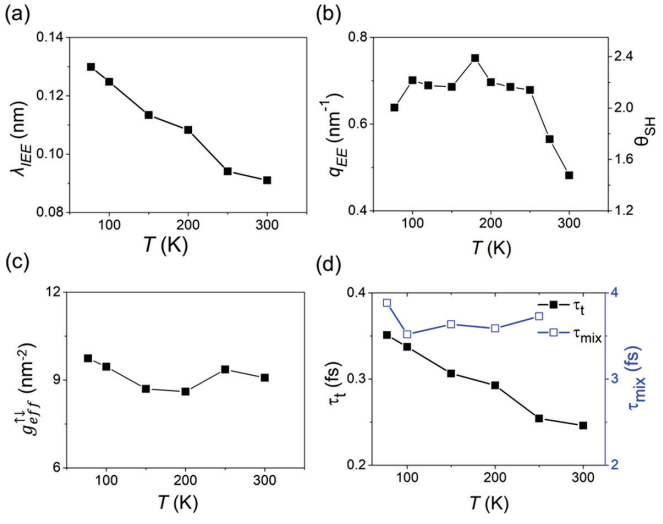

FIG. 4. Temperature-dependent measurements. (a–c) represent λ_{IEE}, q_{EE}, and effective spin mixing conductance as a function of temperature, respectively. (d) Scattering time τ_t at the BST/Ru interface and effective spin mixing time τ_{mix} at the Ru/CoFeB interface as a function of temperature. Both τ_t and τ_{mix} are not strongly dependent on temperature due to the tunneling nature.

problem to a classic metallic interface problem. On the other hand, avoiding direct contact between the TI surface state and metal is crucial for enhancing λ_{IEE}. In the extreme case where τ_t is much larger than τ_{TI}, Eq. (2) gives λ_{IEE} on the order of 100 nm. By this way, previously reported λ_{IEE} with 1000 times difference in BST/MgO/CoFeB (∼100 nm) [47] and BST/NiFe (∼0.1 nm) [36,37] can be explained. This insulating strategy can also be applied to other TI systems such as HgTe [48] or the Rashba 2D gas system [30], where λ_{IEE} can be larger than 10 nm in $SrTiO_3/Al_2O_x$/NiFe [38,49].

In conclusion, TI or more general 2D systems do not suffer from the strict limit $\theta_{SH} < 1$ in 3D systems. Phenomenologically, it is possible to obtain larger than 1 conversion efficiency in either the charge to spin or spin to charge side. We propose a simple but clear physical model to understand the conversion between charge and spin for TI, which is consistent with previous theories and energy conservation law, as well as our experimental results. Based on our understanding, we suggest that enhancing interfacial spin mixing conductance is crucial for a high q_{EE} and avoiding metallic contact is important for enhancing λ_{IEE}.

We acknowledge fruitful discussions with Shufeng Zhang. This work was supported by the NSF Awards No. 1935362, No. 1909416, No. 1810163, and No. 1611570; the Intel Corporation under Contract No. 52318957; and the U.S. Army Research Office MURI program under Grant No. W911NF-16-1-0472.

[1] I. M. Miron, K. Garello, G. Gaudin, P. J. Zermatten, M. V. Costache, S. Auffret, S. Bandiera, B. Rodmacq, A. Schuhl, and P. Gambardella, Perpendicular switching of a single ferromagnetic layer induced by in-plane current injection, Nature (London) **476**, 189 (2011).

[2] L. Liu, C. F. Pai, Y. Li, H. W. Tseng, D. C. Ralph, and R. A. Buhrman, Spin-torque switching with the giant spin Hall effect of tantalum, Science **336**, 555 (2012).

[3] L. Liu, O. J. Lee, T. J. Gudmundsen, D. C. Ralph, and R. A. Buhrman, Current-Induced Switching of Perpendicularly Magnetized Magnetic Layers Using Spin Torque from the Spin Hall Effect, Phys. Rev. Lett. **109**, 096602 (2012).

[4] S. Manipatruni, D. E. Nikonov, and I. A. Young, Beyond CMOS computing with spin and polarization, Nat. Phys. **14**, 338 (2018).

[5] S. Manipatruni, D. E. Nikonov, C. C. Lin, T. A. Gosavi, H. Liu, B. Prasad, Y. L. Huang, E. Bonturim, R. Ramesh, and I. A. Young, Scalable energy-efficient magnetoelectric spin–orbit logic, Nature (London) **565**, 35 (2019).

[6] J. E. Hirsch, Spin Hall Effect, Phys. Rev. Lett. **83**, 1834 (1999).

[7] Y. K. Kato, R. C. Myers, A. C. Gossard, and D. D. Awschalom, Observation of the spin Hall effect in semiconductors, Science **306**, 1910 (2004).

[8] S. O. Valenzuela and M. Tinkham, Direct electronic measurement of the spin Hall effect, Nature (London) **442**, 176 (2006).

[9] J. Sinova, S. O. Valenzuela, J. Wunderlich, C. H. Back, and T. Jungwirth, Spin Hall effects, Rev. Mod. Phys. **87**, 1213 (2015).

[10] E. Saitoh, M. Ueda, H. Miyajima, and G. Tatara, Conversion of spin current into charge current at room temperature: Inverse spin-Hall effect, Appl. Phys. Lett. **88**, 182509 (2006).

[11] T. Kimura, Y. Otani, T. Sato, S. Takahashi, and S. Maekawa, Room-Temperature Reversible Spin Hall Effect, Phys. Rev. Lett. **98**, 156601 (2007).

[12] L. Vila, T. Kimura, and Y. C. Otani, Evolution of the Spin Hall Effect in Pt Nanowires: Size and Temperature Effects, Phys. Rev. Lett. **99**, 226604 (2007).

[13] A. R. Mellnik, J. S. Lee, A. Richardella, J. L. Grab, P. J. Mintun, M. H. Fischer, A. Vaezi, A. Manchon, E. A. Kim, N. Samarth, and D. C. Ralph, Spin-transfer torque generated by a topological insulator, Nature (London) **511**, 449 (2014).

[14] M. Dc, R. Grassi, J. Y. Chen, M. Jamali, D. Reifsnyder Hickey, D. Zhang, Z. Zhao, H. Li, P. Quarterman, Y. Lv, M. Li, A. Manchon, K. A. Mkhoyan, T. Low, and J. P. Wang, Room-temperature high spin–orbit torque due to quantum confinement in sputtered $Bi_xSe_{(1-x)}$ Films, Nat. Mater. **17**, 800 (2018).

[15] N. H. D. Khang, Y. Ueda, and P. N. Hai, A conductive topological insulator with large spin Hall effect for ultralow power spin–orbit torque switching, Nat. Mater. **17**, 808 (2018).

[16] Q. Shao, H. Wu, Q. Pan, P. Zhang, L. Pan, K. Wong, X. Che, and K. L. Wang, Room temperature highly efficient topological insulator/Mo/CoFeB spin-orbit torque memory with perpendicular magnetic anisotropy, in *Proceedings of the 64th Annual IEEE International Electron Devices Meeting, IEDM 2018* (IEEE, San Francisco, 2018).

[17] H. Wu, P. Zhang, P. Deng, Q. Lan, Q. Pan, S. A. Razavi, X. Che, L. Huang, B. Dai, K. Wong, X. Han, and K. L. Wang, Room-Temperature Spin-Orbit Torque from Topological Surface States, Phys. Rev. Lett. **123**, 207205 (2019).

[18] H. Wu, Y. Xu, P. Deng, Q. Pan, S. A. Razavi, K. Wong, L. Huang, B. Dai, Q. Shao, G. Yu, X. Han, J. C. Rojas-Sánchez, S. Mangin, and K. L. Wang, Spin-orbit torque switching of a nearly compensated ferrimagnet by topological surface states, Adv. Mater. **31**, 1901681 (2019).

[19] Y. Fan, P. Upadhyaya, X. Kou, M. Lang, S. Takei, Z. Wang, J. Tang, L. He, L.-T. Chang, M. Montazeri, G. Yu, W. Jiang, T. Nie, R. N. Schwartz, Y. Tserkovnyak, and K. L. Wang, Magnetization switching through giant spin-orbit torque in a magnetically doped topological insulator heterostructure, Nat. Mater. **13**, 699 (2014).

[20] P. Li, J. Kally, S. S. L. Zhang, T. Pillsbury, J. Ding, G. Csaba, J. Ding, J. S. Jiang, Y. Liu, R. Sinclair, C. Bi, A. DeMann, G. Rimal, W. Zhang, S. B. Field, J. Tang, W. Wang, O. G. Heinonen, V. Novosad, A. Hoffmann *et al.*, Magnetization switching using topological surface states, Sci. Adv. **5**, eaaw3415 (2019).

[21] X. Che, Q. Pan, B. Vareskic, J. Zou, L. Pan, P. Zhang, G. Yin, H. Wu, Q. Shao, P. Deng, and K. L. Wang, Strongly surface state carrier-dependent spin–orbit torque in magnetic topological insulators, Adv. Mater. **32**, 1907661 (2020).

[22] P. Deorani, J. Son, K. Banerjee, N. Koirala, M. Brahlek, S. Oh, and H. Yang, Observation of inverse spin Hall effect in bismuth selenide, Phys. Rev. B **90**, 094403 (2014).

[23] Y. Shiomi, K. Nomura, Y. Kajiwara, K. Eto, M. Novak, K. Segawa, Y. Ando, and E. Saitoh, Spin-Electricity Conversion Induced by Spin Injection into Topological Insulators, Phys. Rev. Lett. **113**, 196601 (2014).

[24] K. Kondou, R. Yoshimi, A. Tsukazaki, Y. Fukuma, J. Matsuno, K. S. Takahashi, M. Kawasaki, Y. Tokura, and Y. Otani, Fermi-level-dependent charge-to-spin current conversion by dirac surface states of topological insulators, Nat. Phys. **12**, 1027 (2016).

[25] J. C. Rojas-Sánchez, S. Oyarzún, Y. Fu, A. Marty, C. Vergnaud, S. Gambarelli, L. Vila, M. Jamet, Y. Ohtsubo, A. Taleb-Ibrahimi, P. Le Fèvre, F. Bertran, N. Reyren, J. M. George, and A. Fert, Spin to Charge Conversion at Room Temperature by Spin Pumping into a New Type of Topological Insulator: α-Sn Films, Phys. Rev. Lett. **116**, 096602 (2016).

[26] J. C. R. Sánchez, L. Vila, G. Desfonds, S. Gambarelli, J. P. Attané, J. M. De Teresa, C. Magén, and A. Fert, Spin-to-charge conversion using Rashba coupling at the interface between non-magnetic materials, Nat. Commun. **4**, 1 (2013).

[27] P. Gambardella and I. M. Miron, Current-induced spin-orbit torques, Philos. Trans. R. Soc., A **369**, 3175 (2011).

[28] S. D. Ganichev, E. L. Ivchenko, V. V. Belkov, S. A. Tarasenko, M. Sollinger, D. Weiss, W. Wegscheider, and W. Prettl, Nature (London) **417**, 153 (2002).

[29] S. Zhang and A. Fert, Conversion between spin and charge currents with topological insulators, Phys. Rev. B **94**, 184423 (2016).

[30] R. Dey, N. Prasad, L. F. Register, and S. K. Banerjee, Conversion of spin current into charge current in a topological insulator: Role of the interface, Phys. Rev. B **97**, 174406 (2018).

[31] See Supplemental Material at http://link.aps.org/supplemental/10.1103/PhysRevB.104.L220407 for more derivation, discussion, and experiment details about the spin mixing conductance and also the control experiments without topological insulators.

[32] K. Kondou, H. Tsai, H. Isshiki, and Y. Otani, Efficient spin current generation and suppression of magnetic damping due to fast spin ejection from nonmagnetic metal/indium-tin-oxide interfaces, APL Mater. **6**, 101105 (2018).

[33] H. Isshiki, P. Muduli, J. Kim, K. Kondou, and Y. C. Otani, Phenomenological model for the direct and inverse Edelstein effects, Phys. Rev. B **102**, 184411 (2020).

[34] O. Mosendz, J. E. Pearson, F. Y. Fradin, G. E. W. Bauer, S. D. Bader, and A. Hoffmann, Quantifying Spin Hall Angles from Spin Pumping: Experiments and Theory, Phys. Rev. Lett. **104**, 046601 (2010).

[35] K. Ando, S. Takahashi, J. Ieda, Y. Kajiwara, H. Nakayama, T. Yoshino, K. Harii, Y. Fujikawa, M. Matsuo, S. Maekawa, and E. Saitoh, Inverse spin-Hall effect induced by spin pumping in metallic system, J. Appl. Phys. **109**, 103913 (2011).

[36] J. B. S. Mendes, O. Alves Santos, J. Holanda, R. P. Loreto, C. I. L. de Araujo, C.-Z. Chang, J. S. Moodera, A. Azevedo, and S. M. Rezende, Dirac-surface-state-dominated spin to charge current conversion in the topological insulator $(Bi_{0.22}Sb_{0.78})_2Te_3$ films at room temperature, Phys. Rev. B **96**, 180415(R) (2017).

[37] K. T. Yamamoto, Y. Shiomi, K. Segawa, Y. Ando, and E. Saitoh, Universal scaling for the spin-electricity conversion on surface states of topological insulators, Phys. Rev. B **94**, 024404 (2016).

[38] P. Noël, F. Trier, L. M. Vicente Arche, J. Bréhin, D. C. Vaz, V. Garcia, S. Fusil, A. Barthélémy, L. Vila, M. Bibes, and J. P. Attané, Non-volatile electric control of spin–charge conversion in a $SrTiO_3$ Rashba system, Nature (London) **580**, 483 (2020).

[39] H. He, L. Tai, D. Wu, H. Wu, A. Razavi, K. Wong, Y. Liu, and K. L. Wang, Enhancement of spin-to-charge conversion efficiency in topological insulators by interface engineering, APL Mater. **9**, 071104 (2021).

[40] Y. Tserkovnyak, A. Brataas, and G. E. W. Bauer, Enhanced Gilbert Damping in Thin Ferromagnetic Films, Phys. Rev. Lett. **88**, 117601 (2002).

[41] L. Liu, T. Moriyama, D. C. Ralph, and R. A. Buhrman, Spin-Torque Ferromagnetic Resonance Induced by the Spin Hall Effect, Phys. Rev. Lett. **106**, 036601 (2011).

[42] H. Wang, C. Du, P. C. Hammel, and F. Yang, Antiferromagnonic Spin Transport from $Y_3Fe_5O_{12}$ into NiO, Phys. Rev. Lett. **113**, 097202 (2014).

[43] N. Behera, M. S. Singh, S. Chaudhary, D. K. Pandya, and P. K. Muduli, Effect of Ru thickness on spin pumping in Ru/Py bilayer, J. Appl. Phys. **117**, 17A714 (2015).

[44] J. Zhang, C. Z. Chang, Z. Zhang, J. Wen, X. Feng, K. Li, M. Liu, K. He, L. Wang, X. Chen, Q. K. Xue, X. Ma, and Y. Wang, Band structure engineering in $(Bi_{1-x}Sb_x)_2Te_3$ ternary topological insulators, Nat. Commun. **2**, 574 (2011).

[45] M. Hajlaoui, E. Papalazarou, J. Mauchain, G. Lantz, N. Moisan, D. Boschetto, Z. Jiang, I. Miotkowski, Y. P. Chen, A. Taleb-Ibrahimi, L. Perfetti, and M. Marsi, Ultrafast surface carrier dynamics in the topological insulator Bi_2Te_3, Nano Lett. **12**, 3532 (2012).

[46] T. Zhang and G. Y. Guo, Density-functional theory calculation of electronic and magnetic properties of hexagonal V/Ru thin films and superlattices, Phys. Rev. B **71**, 214442 (2005).

[47] L. Liu, A. Richardella, I. Garate, Y. Zhu, N. Samarth, and C. T. Chen, Spin-polarized tunneling study of spin-momentum locking in topological insulators, Phys. Rev. B **91**, 235437 (2015).

[48] P. Noel, C. Thomas, Y. Fu, L. Vila, B. Haas, P. H. Jouneau, S. Gambarelli, T. Meunier, P. Ballet, and J. P. Attané, Highly Efficient Spin-to-Charge Current Conversion in Strained HgTe Surface States Protected by a HgCdTe Layer, Phys. Rev. Lett. **120**, 167201 (2018).

[49] D. C. Vaz, P. Noël, A. Johansson, B. Göbel, F. Y. Bruno, G. Singh, S. McKeown-Walker, F. Trier, L. M. Vicente-Arche, A. Sander, S. Valencia, P. Bruneel, M. Vivek, M. Gabay, N. Bergeal, F. Baumberger, H. Okuno, A. Barthélémy, A. Fert, L. Vila *et al.*, Mapping spin–charge conversion to the band structure in a topological oxide two-dimensional electron gas, Nat. Mater. **18**, 1187 (2019).